Available online at www.sciencedirect.com

jmr&t Journal of Materials Research and Technology

journal homepage: www.elsevier.com/locate/jmrt

Effect of minor gallium addition on corrosion, passivity, and antibacterial behaviour of novel β-type Ti–Nb alloys

Adnan Akman [a,*], *Ludovico Andrea Alberta* [a], *Paula Milena Giraldo-Osorno* [b,c], *Adam Benedict Turner* [b,c], *Martin Hantusch* [a], *Anders Palmquist* [b], *Margarita Trobos* [b,c], *Mariana Calin* [a], *Annett Gebert* [a]

[a] *Leibniz Institute for Solid State and Materials Research, Helmholtzstr. 20, D-01069 Dresden, Germany*
[b] *Department of Biomaterials, Institute of Clinical Sciences, Sahlgrenska Academy University of Gothenburg, Gothenburg, Sweden*
[c] *Centre for Antibiotic Resistance Research in Gothenburg (CARe), University of Gothenburg, Gothenburg, Sweden*

ARTICLE INFO

Article history:
Received 26 April 2023
Accepted 23 June 2023
Available online 27 June 2023

Keywords:
β titanium alloy
Gallium
Corrosion
Passive film
Antibacterial
Cytocompatibility

ABSTRACT

Metastable Ti–Nb alloys are promising bone-implant materials due to improved mechanical biofunctionality and biocompatibility. To overcome increasing bacterial infection risk, alloying with antibacterial elements is a promising strategy. This study investigates the effect of minor gallium (Ga) additions (4, 8 wt% Ga) to as-cast and solution-treated β-type Ti–45Nb-based alloy (96(Ti–45Nb)-4Ga, 92(Ti–45Nb)-8Ga (wt.%)) on corrosion and passive film properties, as well as cytocompatibility and antibacterial activity. The electrochemical properties were evaluated by potentiodynamic polarization, electrochemical impedance spectroscopy (EIS), and Mott-Schottky analyses in phosphate-buffered saline (PBS). X-ray photoelectron spectroscopy (XPS) was performed to analyze the chemical composition of passive films. Early adhesion and viability of macrophages and *Staphylococcus aureus* were assessed by nucleocounting and colony-forming unit counting, respectively. The results showed that high corrosion resistance and passive film properties of Ti–45Nb are retained and even slightly improved with Ga. EIS results revealed that Ga addition improves the passive film resistance. XPS measurements of 92(Ti–45Nb)-8Ga show that the passive film contains Ti-, Nb- and Ga-based oxides, implying the formation of mixed (Ti–Nb-Ga) oxides. In addition, marginal Ga ion release rate was detected under free corrosion conditions. Therefore, it can be assumed that Ga species may contribute to passive film formation on Ga-containing alloys. The 92(Ti–45Nb)-8Ga elicited an antibacterial effect against *S. aureus* compared to cp-Ti at 4 h. Moreover, Ga-containing alloys showed good cytocompatibility with THP-1 macrophages at 24 h. In conclusion, it was demonstrated that Ga additions to Ti–45Nb are beneficial to corrosion resistance and showed promising initial host and bacterial interactions.

* Corresponding author.
E-mail addresses: a.akman@ifw-dresden.de (A. Akman), l.a.alberta@ifw-dresden.de (L.A. Alberta), paula.giraldo@biomaterials.gu.se (P.M. Giraldo-Osorno), adam.turner@biomaterials.gu.se (A.B. Turner), m.hantusch@ifw-dresden.de (M. Hantusch), anders.palmquist@biomaterials.gu.se (A. Palmquist), margarita.trobos@biomaterials.gu.se (M. Trobos), m.calin@ifw-dresden.de (M. Calin), a.gebert@ifw-dresden.de (A. Gebert).
https://doi.org/10.1016/j.jmrt.2023.06.219

1. Introduction

Titanium alloys are widely used as materials for hard-tissue implants due to their high corrosion resistance and excellent biocompatibility compared to other commercial metallic implant materials (*e.g.,* Co–Cr, austenitic stainless steel) [1,2]. However, the most widely used biomedical Ti alloys (Ti–6Al–4V, Ti–6Al–7Nb) have drawbacks that could lead to implant failure. These alloys exhibit higher elastic moduli ($E = 105–114$ GPa), compared to cortical bone ($E = 10–30$ GPa). This mismatch between the implant and the surrounding bone leads to the aseptic loosening of load-bearing implants (known as a stress shielding phenomenon) [3,4]. In addition, long-term studies have shown the development of health disorders due to the release of metallic ions including aluminium and vanadium into the surrounding tissues and bloodstream [5–8].

Another major cause of implant failure is biomaterial-associated infection, suggested to originate when bacterial biofilms form on implant surfaces and the innate immune response fails to eradicate them [9]. Moreover, bacteria in biofilms are difficult to treat as they exhibit increased resistance to antibiotics compared to their planktonic (free-floating) counterparts [9,10]. For Ti alloys, biofilm formation can be inhibited by coating or alloying the implant with inorganic antibacterial agents such as Zn, Ag, Cu, and Ga [11–13]. Ga (III)-based compounds have shown antibacterial activity on infections caused by multidrug-resistant ESKAPE pathogens (*Enterococcus faecium, Staphylococcus aureus, Klebsiella pneumoniae, Pseudomonas aeruginosa, and Enterobacter species*) [14], and against *P. aeruginosa* biofilms [15]. Ga (in Ga^{3+} form) has the potential to reduce bacterial viability and biofilm formation on implant surfaces without the use of antibiotics [12]. Due to its biochemical similarity with iron (Fe), Ga can disrupt bacterial iron metabolism [16]. Ga substitutes Fe in siderophore-dependent biological processes (*i.e.,* bacterial Fe scavenging and transport systems, and enzyme synthesis pathways) [15], resulting in the release of Fenton-active Fe into the cytoplasm and generation of reactive oxygen species. In addition to the desired antibacterial effect, it is important that antibacterial modifications of biomaterial surfaces retain good biocompatibility with host cells and tissues, as well as promote the host immune response [16,17].

Recently, β-type Ti alloys have gained attention for implant applications due to the combination of low elastic modulus with appropriate strength. A special focus is on β-type Ti–Nb based alloys which exhibit elastic modulus values of 60–69 GPa, much lower than clinically used implant materials like cp-Ti and Ti–6Al–4V [18–22]. In addition to the attractive mechanical properties, excellent corrosion performance has been demonstrated due to the formation of a uniform and stable passive film as Ti- and Nb-based mixed oxide on the surface of β-type Ti–Nb alloys [23–29]. The corrosion behaviour and passive film characteristics of metallic implants are critical since they can lead to metal ion release from the implant to surrounding tissues causing metal toxicity [30,31]. This adverse consequence of the corrosion phenomena can be prevented or inhibited by passivation and re-passivation, therefore, controlling the corrosion initiation and propagation [32,33].

The electrochemical response of β-type alloys such as Ti–29Nb–13Ta-4.6Zr [34], Ti-33.5Nb-5.7Ta [35] or Ti–13Nb–13Zr [36,37] has been studied in physiological solutions and high corrosion resistance was confirmed. Woldemedhin et al. [24] studied the characterization of the anodic oxides of Ti–Nb alloys (Nb content 10 and 20 wt%) via cyclic voltammetry, electrochemical impedance spectroscopy (EIS) and Mott-Schottky analysis. The cyclic voltammetry results revealed that anodic oxides grow under a high-field growth mechanism. In addition, a linear relationship was found between the inverse capacitance of the anodic oxides and the applied potential, which means that the oxides are dielectric. Gebert and Gostin et al. [38] investigated corrosive metal release, passivity, and bone cell response of β-type Ti–40Nb under different surface treatment conditions. Results revealed that Nb species are involved in the oxidation processes by forming Ti–Nb mixed oxide. Gebert et al. [19] investigated the effect of indium (In) alloying addition on the corrosion properties of Ti–40Nb in Ringer solution. Indium (In) can form soluble chloro-complexes in Ringer solution, but minor additions of In up to 4 wt% did not cause substantial corrosive metal release due to the formation of barrier-type Ti- and Nb-oxide films with small In-oxide/hydroxide fractions and with indium (In) addition, a remarkable decrease in elastic modulus was observed (down to ≤ 50 GPa) [21].

Recently, Alberta et al. [20] studied the effect of Ga and Cu addition on the mechanical properties of novel low elastic modulus β-type Ti–45Nb alloys for antibacterial implant applications. As an alloying addition, Ga and Cu were chosen due to their antibacterial properties to be used to tackle implant-associated infections. Results showed that a small addition of Ga and Cu increased the yield strength under compression and tension with higher elastic energy than Ti–45Nb (due to the grain boundary and solid-solution strengthening effect). In addition, elastic modulus values of the studied alloys including Ti–45Nb are in the range of 64–79 GPa, *i.e.* lower than those of clinically used alloys ($E = 105–114$ GPa) [39].

Though Ga is proposed as a potential bactericidal alloying addition for Ti-based materials, the Ga-related reaction paths at an implant alloy-body fluid interface are still not understood in detail. It is essential to understand the implant alloy-body fluid interactions due to the changes in the surface chemistry of the implants under body fluids. The present study aims to elucidate the role of Ga (4 and 8 wt%) in (i) the corrosion reactivity and passive film formation of a β-type

Ti–Nb alloy in physiological conditions and (ii) the early direct material-cell interactions with macrophages and *S. aureus in vitro*.

2. Materials and methods

2.1. Material and microstructural characterization

Cylindrical samples (rods) of nominal compositions 96(Ti–45Nb)-4Ga, 92(Ti–45Nb)-8Ga (wt.%) were prepared by casting methods in two steps, starting from commercially available Ti–45Nb alloy (99.9% ASTM B348-13) and high purity Ga (99.99%). First, button-shaped ingots were obtained by arc-melting. Then, the ingot materials were cast into a rod shape, using a cold crucible levitation device with water-cooled copper moulds (10 mm diameter). The as-cast rods were subjected to β-solution treatment at 1000 °C for 24 h, followed by water quenching. For the present study, the developed alloys were compared with the solution-treated Ti–45Nb alloy. Microstructural characterization of the alloys was conducted by transmission X-ray diffraction (XRD) and scanning electron microscopy (SEM). Comprehensive information about the alloy preparation, chemical composition analysis, and microstructural characterization is provided elsewhere [20,40,41].

2.2. Electrochemical measurements

Electrochemical experiments were employed to investigate the effect of minor Ga addition on the corrosion and passive film properties of β-type Ti–Nb alloys. The alloy samples were mechanically ground with SiC emery paper (from grit 320 to 4000) and cleaned with ethanol. Prior to electrochemical measurements, the alloy samples were electronically contacted with copper tape. Electrochemical measurements were performed in a phosphate-buffered saline (PBS) solution (NaCl 140 mM, KCl 3 mM, phosphate buffer 10 mM with a pH of 7.4, Merck KGaA). A Solartron XM ModuLab potentiostat was used in combination with a three-electrode Teflon cell. Studied alloys were used as the working electrode (effective electrode area of 0.385 cm^2), and a platinum (Pt) net was used as the counter electrode. The potentials were measured versus the saturated calomel electrode (SCE, E(SCE) = 241 mV vs. SHE (standard hydrogen electrode)) as the reference electrode. The electrochemical tests were repeated three times to ensure data reproducibility and the obtained data from electrochemical experiments were represented with error limits (standard deviation). To determine the corrosion response of the samples, the open circuit potential (OCP) was measured for 1 h. Then, a potentiodynamic polarization measurement was conducted in a potential range between −0.2 V (vs. OCP) to 1 V (vs. SCE) with a scan rate of 0.5 mV/s. ECLab software (v11.36) was used to analyze the data from polarization measurements.

For analyzing the passive film growth, potentiostatic anodic polarization tests were conducted at 0.6 V (vs. SCE) for 1 h, at which steady-state current density was observed for all samples. Then, electrochemical impedance spectroscopy (EIS) measurements were carried out to investigate the electrochemical response of the potentiostatic pre-passivated films. EIS measurements were conducted by applying an alternating current (AC) perturbation in the frequency range from 10 kHz to 10 mHz with a 10 mV amplitude. Zview 4 software was used for analyzing the impedance data. After EIS measurements, capacitance measurements (Mott-Schottky analysis) were performed to characterize the electronic properties of the passive films formed at 0.6 V (vs. SCE). Capacitance measurements were carried out by applying an AC perturbation at a fixed frequency of 1 kHz. A potential range of 1 V (vs. SCE) to −1 V (vs. SCE) was swept with a step size of 50 mV.

2.3. Metal ion release analysis

Metal ion release studies were conducted with an iCAP 6500 Duo View inductively coupled plasma optical emission spectroscopy (ICP-OES) device on Ti–45Nb and 92(Ti–45Nb)-8Ga samples in PBS solution at 37.5 °C for 7 days based on DIN EN ISO 10993–15 (10/2009). Mechanically ground (up to grit 2400) specimens were carefully rinsed in distilled water and subsequently in pure ethanol for 15 min using an ultrasonic bath, then dried at room temperature and stored in a vacuum prior to testing. Each solution was diluted 1:3 with distilled water. Three samples per material and three blanks were tested. Comprehensive information about the test procedure was provided elsewhere [19].

2.4. Passive film analysis

X-ray photoelectron spectroscopy (XPS) experiments were performed to investigate the chemical composition of the passive films formed via potentiostatic polarization at 0.6 V (vs. SCE) for 1 h (air-exposed samples were used as reference). A PHI 5600 (Physical Electronics) spectrometer with an Al K-alpha monochromatic X-ray source (200 W) was employed to collect XPS spectra. The chosen take-off angle and X-ray spot size were 45 ° and 800 μm for high-resolution scans, respectively. MultiPak software was used for fitting the acquired XPS data. Comprehensive information about the passive film analysis was provided elsewhere [19].

2.5. THP-1 macrophage viability and adhesion

To evaluate the potential effect of the β-type Ti–Nb alloys as implanted biomaterial, the *in vitro* response of the human monocytic cell line THP-1 (ATCC, Manassas, USA) was evaluated by direct seeding onto Ti–45Nb, 96(Ti–45Nb)-4Ga, 92(Ti–45Nb)-8Ga and control commercially pure titanium (cp-Ti grade IV, Christers Finmekaniska AB, Skövde, Sweden). The discs were sterilized by immersion in 70% ethanol for 20 min followed by washing three times with sterile water and allowing them to air-dry.

THP-1 was grown in Roswell Park Memorial Institute (RPMI) 1640 medium supplemented with 10% FBS, 0.5% β-mercaptoethanol (Sigma Aldrich, Munich, Germany) and 1% penicillin/streptomycin (PEST) solution (Gibco Life Technologies, Carlsbad, California USA) in a 37 °C humidified incubator with 5% CO_2. Cells in passage 6 were used. Media was changed every two days. THP-1 monocytes were stimulated with 10 ng/

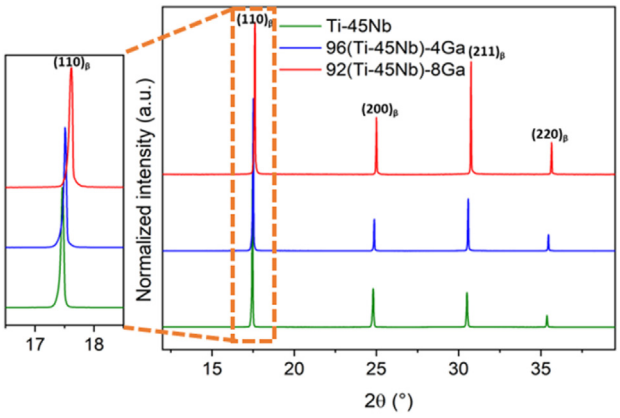

Fig. 1 – X-ray diffractograms of Ti–45Nb, 96(Ti–45Nb)-4Ga, 92(Ti–45Nb)-8Ga alloy samples in solution-treated states with a magnified view of the most dominant diffraction peak.

mL phorbol-12-myristate-13-acetate (PMA, Sigma Aldrich, Munich, Germany) for 48 h to induce macrophage differentiation, followed by 24 h of resting time in fresh media without PMA. THP-1 differentiated macrophages were detached with trypsin (Gibco Life Technologies, Waltham, USA), and seeded on the material discs (in duplicates) at a density of 700 000 cells/mL in 48-well plates (Nunc, Thermo Fisher Scientist, Roskilde, Denmark). After 24 h of direct cell contact with the surface, the number of viable cells adhered to the surface was quantified using a NucleoCounter® NC-200TM system (ChemoMetec A/S, Lillerød, Denmark). The experiment was repeated three times (n = 3).

2.6. Staphylococcus aureus *viability and adhesion*

The material discs were sterilized in ethanol as described above. *Staphylococcus aureus* ATCC 25923 (American Type Culture Collection, Manassas, USA) was streaked from a 80 °C frozen stock onto 5% horse blood Columbia agar (HBA, Media Department, Clinical Microbiology Laboratory, Sahlgrenska University Hospital, Sweden) and incubated at 37 °C overnight. Single colonies were collected and inoculated into tryptic soy broth (TSB, Scharlau, Barcelona, Spain) to achieve an OD_{546} of 0.13, equivalent to 10^8 CFU/mL, and further diluted (1:1000) to 10^5 CFU/mL. One mL of *S. aureus* suspension (10^5 CFU/mL) was added to each well of a 48-well plate (Nunc, Thermo Fisher Scientific, Waltham, USA) containing either a control cp-Ti disc or one of the test materials (96(Ti–45Nb)-4Ga or 92(Ti–45Nb)-8Ga) (in duplicates) and incubated statically at 37 °C for either 4 or 24 h to assess the role of Ga on bacterial viability. Upon completion of the incubation period, *S. aureus* cells adhered to the surfaces were detached and disaggregated by transferring the discs to a 15 mL Falcon tube containing 1 mL saline (0.9%) and sonicating (42 kHz) in an ultrasonic cleaner (Branson 3510 MT, Brookfield, CT, USA) for 30 s followed by vortexing at 10 000 rpm for 1 min. A volume of 100 μL of the detached and disaggregated bacterial cells was ten-fold serially diluted in saline (0.9%) and Triton-X (0.1%), from which 5 μL were plated on HBA plates and incubated at 37 °C overnight, before the enumeration of viable colony-forming units (CFU). The experiment was repeated three times (n = 3).

2.7. *Statistics*

All biological quantitative data were analyzed with GraphPad Prism 9 (GraphPad Software Inc., San Diego, CA, USA) and presented as the mean ± standard deviation. For the cytocompatibility and bacterial viability analysis, statistical differences were assessed by one-way analysis of variance (ANOVA) with LSD multiple comparisons between Ti–45Nb, 96(Ti–45Nb)-4Ga, and 92(Ti–45Nb)-8Ga. Dunnett's post-hoc was used to compare each of the test β-type Ti–Nb alloys to the clinically relevant cp-Ti control. A value of $p < 0.05$ was considered statistically significant.

3. Results

3.1. *Microstructural characterization*

Before starting corrosion analyses, microstructural investigations on the cast and solution-treated alloys (96(Ti–45Nb)-4Ga, 92(Ti–45Nb)-8Ga (wt.%)), in comparison to Ti45Nb, were performed. The X-ray diffraction patterns of the alloy sample types after solution treatment are shown in Fig. 1, revealing for all a β-phase structure with no diffraction peaks which could be indicative of secondary phases (*e.g.*, α′, α″, ω). This is due to the stabilizing effect of the high Nb fractions on the β-phase [42]. SEM images of the alloy microstructures obtained after solution treatment and water-quenching are shown in Fig. 2. All three alloys consist of equiaxed β-grains with various grain sizes. The average grain size reaches 55 μm when Ga content is 4 wt% and then it

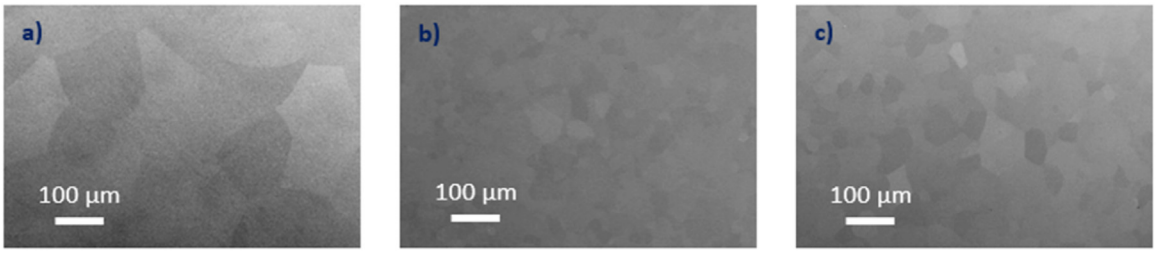

Fig. 2 – SEM micrographs taken from cross-sectional regions of a) Ti–45Nb, b) 96(Ti–45Nb)-4Ga and c) 92(Ti–45Nb)-8Ga rod samples in solution-treated states.

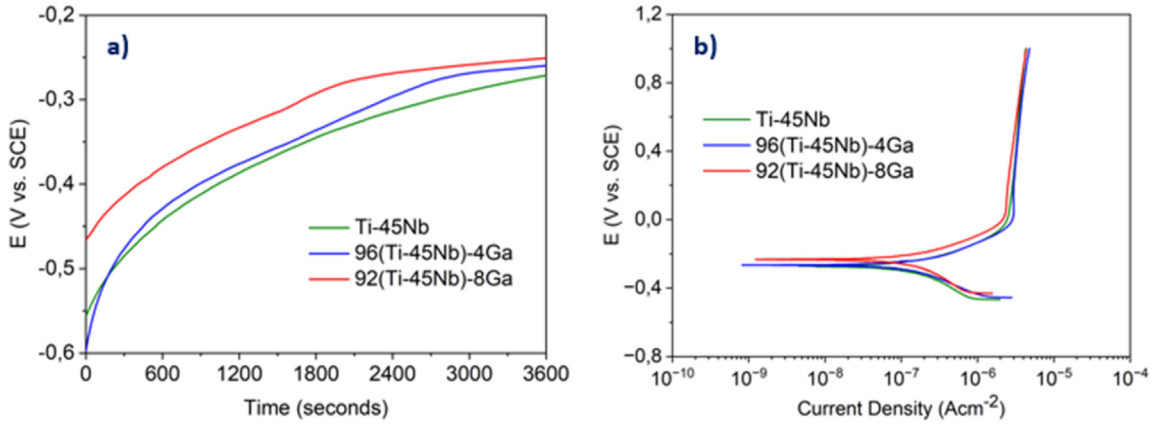

Fig. 3 – a) Open circuit potential transients recorded during 1 h of immersion in PBS. b) Potentiodynamic polarization curves of the alloy samples in PBS solution.

increases to 141 μm when Ga content is 8 wt%. Grain refinement was observed for Ga-containing alloys and the refinement could be attributed to reduced atomic mobility during casting & solution treatment which slows down the growth of equiaxed β-grains [41]. Further comprehensive information about the chemical composition and microstructural features of the alloys has been provided previously [20,40,41].

3.2. Electrochemical characterization

Open Circuit Potential (OCP) – Fig. 3a shows exemplary open circuit potential transients recorded for Ti–45Nb and 96(Ti–45Nb)-4Ga, 92(Ti–45Nb)-8Ga alloys in PBS solution. For all alloys, the open circuit potentials shift to a more positive direction (increment of the potential over time) which is indicative of the spontaneous passive film formation. The nearly steady state OCP values for Ti–45Nb and 96(Ti–45Nb)-4Ga, 92(Ti–45Nb)-8Ga alloy samples in PBS solution after 1 h are −282 ± 20 mV, −205 ± 37 mV, and −226 ± 30 mV (vs. SCE), respectively. The potential difference between Ti–45Nb and the Ga-containing samples can be explained by the difference in the redox potential of individual metals. The redox potential for Ga (Ga/Ga^{3+} (−0.56 V vs. SHE)) is more positive than the redox potential of Ti (Ti/Ti^{2+} (−1.63 V vs. SHE)) and Nb (Nb/Nb^{5+} (−1.09 V vs. SHE)) [43,44]. Thus, due to the presence of Ga content in the solid solution [40], Ga-containing alloys exhibit more positive OCP values compared to Ti–45Nb. However, considering the error limits of the method, no significant difference is observed among the Ga-containing ones.

Potentiodynamic polarization – Potentiodynamic polarization experiments were conducted in PBS solution after 1 h of OCP at which steady state is achieved, as shown in Fig. 3b. All tested Ti alloys exhibit similar polarization behaviour with an initial low current density level at the corrosion potential (E_{corr}), indicative of low corrosion activity and stable anodic passive film formation in a potential range between 0.1 V (vs. SCE) to 1 V (vs. SCE). Nearly steady-state passivation current densities in the range of a few $\mu A/cm^2$ were measured which is a characteristic response for valve metals (Ti, Nb, Ta, Al) [45]. In addition, for the Ga-containing alloys, no passive layer breakdown was detected.

Tafel extrapolations were applied to potentiodynamic polarization curves to calculate values for corrosion current density (i_{corr}) and corrosion potential (E_{corr}). A passive film formation potential was selected at 0.6 V (vs. SCE) corresponding to a characteristic passive current density (i_{pass}). The determined values are given in Table 1. The E_{corr} values are shifted to more positive values (increment of the potential over time) with Ga addition. As explained above for OCP values, the redox potential for Ga is more positive than the redox potential of Ti and Nb. Thus, Ga-containing alloys exhibit higher E_{corr} values compared to the Ti–45Nb reference. However, no significant E_{corr} difference was observed among Ga-containing alloys. In addition, i_{corr} values are very low, *i.e.*, in the range of a few tenths of nA/cm^2. But they are slightly higher for Ti–45Nb compared to the Ga-containing ternary alloys, whereas no significant difference is observed among Ga-containing ones. Since there is a direct correlation between i_{corr} and the released metal ions from the electrode surface, it is possible to assume that, Ga-containing alloys do not show evidence for significant Ga ion release due to lower i_{corr} values.

To scrutinize this statement, metal ion release tests were performed on Ti–45Nb and 96(Ti–45Nb)-8Ga samples in PBS

Table 1 – Open circuit potential (E_{OCP}), corrosion current density (i_{corr}), passivation current density (i_{pass}) (at 0.6 V (vs. SCE)), corrosion potential (E_{corr}) and polarization resistance (R_p) values obtained for Ti–45Nb and 96(Ti–45Nb)-4Ga, 92(Ti–45Nb)-8Ga alloys from potentiodynamic polarization experiments. Potential values are reported vs. SCE (E(SCE) = 241 mV vs. SHE).

	E_{OCP} (mV)	E_{corr} (mV)	i_{corr} (μAcm^{-2})	i_{pass} (μAcm^{-2})	R_p ($k\Omega cm^2$)
Ti–45Nb	−282 ± 20	−282 ± 18	0.07 ± 0.02	3.9 ± 0.6	312 ± 62
96(Ti–45Nb)-4Ga	−205 ± 37	−230 ± 38	0.03 ± 0.01	2.5 ± 0.5	560 ± 99
92(Ti–45Nb)-8Ga	−226 ± 30	−238 ± 27	0.04 ± 0.01	3.2 ± 0.6	418 ± 54

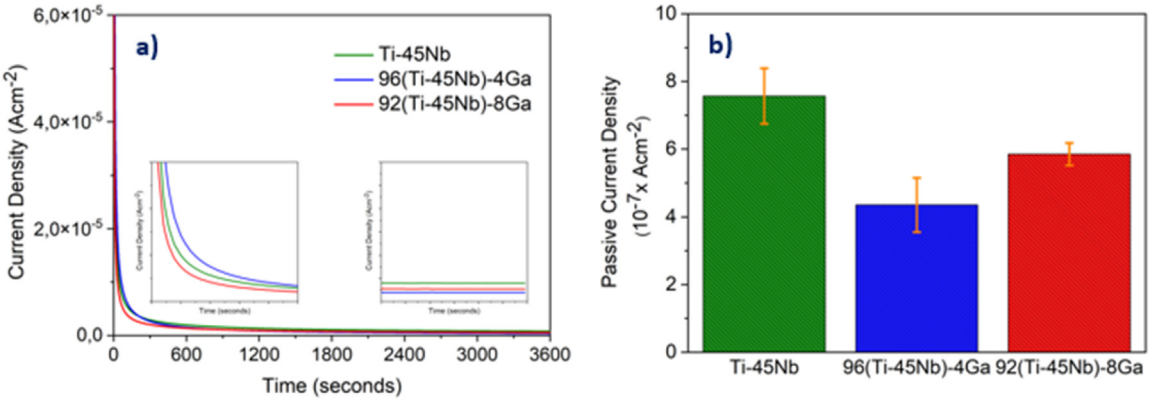

Fig. 4 – a) Current density vs time curves during potentiostatic polarization at 0.6 V (vs. SCE) in PBS solution with an inset showing the current transition in the first 100 s and last 60 s. b) Mean passive current density values (calculated from the last minute of current density vs time curve) after 1 h of potentiostatic polarization for Ti–45Nb and 96(Ti–45Nb)-4Ga, 92(Ti–45Nb)-8Ga alloys in solution-treated states.

solution at 37.5 °C for 7 days. For both alloys, released concentrations of Ti and Nb species remained below the limit of quantification (LOQ) at $7x10^{-8}$ mmol/cm^2. For 96(Ti–45Nb)-8Ga, the concentration of Ga species in solution was detected as $3.5x10^{-7}$ mmol/cm^2, moderately above the LOQ of Ga at $2.5x10^{-7}$ mmol/cm^2. This confirms a very low Ga release rate even after long exposure under free corrosion conditions. Therefore, it can be assumed that Ga species may contribute to the passive film formation on those Ti–Nb-Ga alloy surfaces rather than to corrosive ion release. Thus, the next steps aimed to understand how Ga-based oxides can contribute to passivity states in addition to known Ti- and Nb-based oxide contributions [19,23,27]. The i_{pass} values are lower for Ga-containing alloys than for Ti–45Nb, indicating further depletion of the electronic and/or ionic conductivity of their passive films compared to those on the binary alloy. However, it is not possible to observe a direct trend for i_{pass} values with Ga addition. The i_{pass} values are slightly lower for 96(Ti–45Nb)-4Ga than 92(Ti–45Nb)-8Ga. The potential-pH equilibrium diagram for the pure Ga–H_2O system can be used as a predictive tool to derive information about the contribution of Ga species to passive films. The diagram reveals a quite wide region from pH = 3 to pH = 11.5 with thermodynamically stable Ga-based oxides, mainly Ga_2O_3, in the stability range of water [46]. Accordingly, above −0.8 V (vs. SHE) at a pH value of 7.4, Ga-based oxides can be expected to contribute to the ternary alloy passivity in addition to Ti- and Nb-based oxides (though passive layer formation is also determined by kinetic and structural factors) [19]. In addition, polarization resistance (R_p) values were calculated from the Stern-Geary equation [47] after calculating the anodic and cathodic slopes via Tafel extrapolation. Ga-containing alloys exhibit higher R_p values than Ti–45Nb. However, no significant R_p difference was observed among Ga-containing ones.

Potentiostatic polarization – Potentiostatic polarization measurements were conducted to study the passive film properties. Fig. 4a shows the current density transients of the alloys during anodic potentiostatic polarization at 0.6 V (vs. SCE). The sharp decrease in current density in the first few seconds represents the formation of the passive film after the double-layer re-charging. The current density reaches a nearly stable value with further polarization (passive film resistance increases with the decrease in the current densities). In valve metal theory, surfaces of the valve metals (Ti, Nb, Al, Ta) are usually covered by barrier-type oxide films which possess electronic and ionic conductivity in

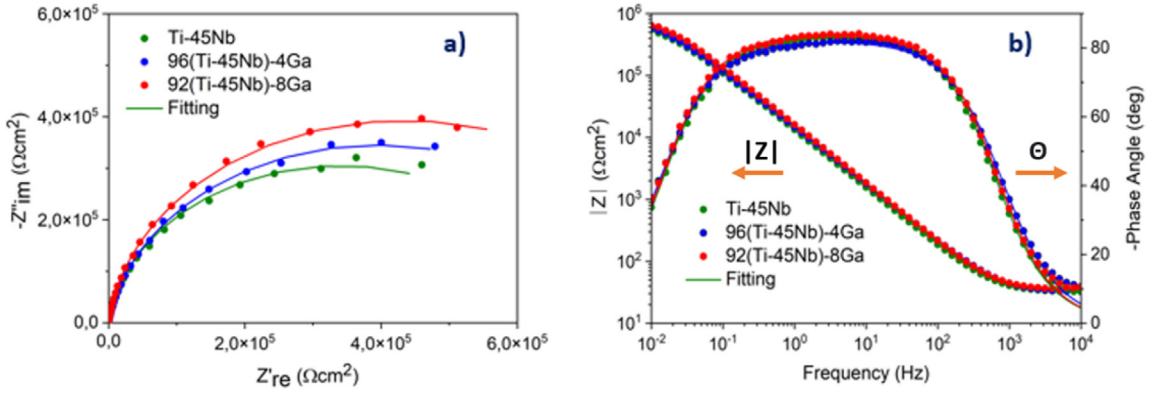

Fig. 5 – EIS measurements - a) Nyquist plot and b) Bode plot of Ti–45Nb and 96(Ti–45Nb)-4Ga, 92(Ti–45Nb)-8Ga alloys; prior to measurements, samples were passivated at 0.6 V (vs. SCE) for 1 h in PBS solution.

dependence on high electric field strength. In our case, the electrochemical response of the alloys is mainly governed by the strong passivating nature (non/low conductive) due to the major contribution of Ti and Nb to passivation [19,45,48]. It is observed that the mean current density values (mean current density is calculated from the last minute of current density vs time curve) for Ga-containing alloy samples are lower than Ti–45Nb after 1 h of potentiostatic polarization, as shown in Fig. 4b. The change in i_{pass} with Ga-content is congruent with that observed in the passive region of potentiodynamic polarization curves (Fig. 3b). The difference in mean passive current density values between Ti–45Nb and Ga-containing alloys suggests that the conductivity/permeability for charge carriers of passive films grown on Ti–45Nb is higher than of the passive film formed on 96(Ti–45Nb)-4Ga, 92(Ti–45Nb)-8Ga samples. Thus, the passive film of Ga-containing alloy surfaces provides higher barrier properties than Ti–45Nb. However, it is not possible to observe a direct trend for current density values with Ga addition. In addition, for Ga-containing alloys, the reduction in current densities could be attributed to the size of β-grains since grain size affects the electrochemical properties [49]. However, the literature reports different results for the effect of grain size on the corrosion behaviour of titanium alloys, from the higher to the lower corrosion resistance [49–52]. In our case, it might be possible to expect lower current density values for 96(Ti–45Nb)-4Ga (wt.%) since the average grain size reaches a minimum of 55 μm when Ga content is 4 wt% compared to 92(Ti–45Nb)-8Ga (wt.%) [41].

Electrochemical Impedance Spectroscopy (EIS) – In this work, EIS is used to evaluate the electrochemical response of the passive film formed under anodic potentiostatic polarization. Fig. 5 shows representative EIS spectra for the studied alloys. Before EIS measurements, potentiostatic anodic polarization for passive film formation was conducted at 0.6 V (vs. SCE) in PBS solution for 1 h.

The radius of the semi-circle in the Nyquist plots (Fig. 5a) indicates the impedance of the passive films grown under potentiostatic anodic polarization. In principle, the higher impedance of the passive film, the larger the Nyquist circle radius. In addition, for the Bode plot (Fig. 5b), the high-frequency range (where the phase angle drops to values near zero between 10^4 Hz to 10^3 Hz) represents the solution resistance of the electrolyte. At the intermediate frequency range (10^3 Hz to 10^{-1} Hz), the absolute phase angle values rise. At low frequencies (10^{-1} Hz to 10^{-2} Hz), the phase angle plot decreases to lower values which represents the behaviour of the passive film [53,54]. All alloys behaved similarly during impedance measurements in terms of the shape of the Nyquist (Fig. 5a) and Bode plots (Fig. 5b). However, the semi-circle radius in the Nyquist plots and the Bode impedance modulus values (|Z|, at the lowest frequency of 10^{-2} Hz) were increased with minor Ga additions. This could be attributed to the contribution of Ga-based oxides to passive film growth together with Ti- and Nb-based oxides.

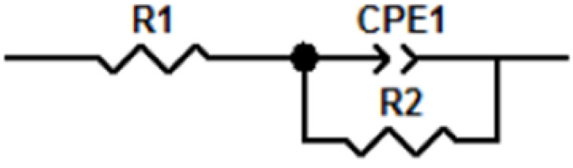

Fig. 6 – The equivalent electrical circuit for modelling the electrochemical response of anodically pre-passivated Ti–45Nb, 96(Ti–45Nb)-4Ga and 92(Ti–45Nb)-8Ga alloys.

The equivalent electrical circuit (EEC) fitting of the impedance data was performed with a circuit as shown in Fig. 6, with a constant phase element (CPE) instead of an ideal capacitor [45,53,54]. The deviation from the ideal capacitive response can be attributed to the heterogeneities and/or roughness in the passive film [55,56]. In the EEC, R_1 represents the resistivity of the electrolyte, R_2 and CPE_1 are related to the resistive and capacitive response of the passive film, respectively. As mentioned above for Bode plots, the high-frequency range represents the solution resistance of the electrolyte (R_1). At low frequencies, the phase angle plot decreases to lower values, which represents the electrochemical behaviour of the passive film (R_2 and CPE_1). The calculated resistance and capacitance values after the circuit fitting are shown in Table 2.

From the equivalent electrical circuit fitting results, it is possible to make comments about Ga addition on the electrochemical response of the alloys. The minor addition of Ga slightly improves the passive film resistance (R_2) of the alloys as seen in Table 2. In addition, impedance modulus values (from Bode plot) were obtained, 518.51 ± 20.92 kΩcm^2 for Ti–45Nb and 556.91 ± 44.85 kΩcm^2, 644.13 ± 23.59 kΩcm^2 for 96(Ti–45Nb)-4Ga, 92(Ti–45Nb)-8Ga respectively, at the lowest frequency of 10^{-2} Hz. As a result of the EIS measurements, the arc diameter of the Nyquist plots and the impedance modulus at the lowest frequency was increased with minor Ga additions (passive film resistance improved). The results from EIS measurements are not in total agreement with the trends of passive current densities observed at potentiostatic polarization measurements and potentiodynamic polarization curves (Figs. 3 and 4). In terms of overall electrochemical response, it is not possible to observe a direct trend with Ga addition, but both Ga-containing alloys exhibit better protective passive film properties compared to the reference Ti–45Nb. In addition, CPE_1-n values of all alloys showed similar capacitive behaviour of around 0.9. It means that the electrochemical response of the passive film formed on the alloys slightly deviates from the pure capacitive (CPE_1-$n = 1$) behaviour (where (CPE_1-$n = 0$) describes a perfect resistor).

Capacitance measurements – Mott-Schottky analysis is used to understand the phenomena occurring at the interface of a passive film (as a semiconductor) and the electrolyte [57]. The analysis was performed here to characterize the semiconductive behaviour of the passive films grown at 0.6 V (vs. SCE) in PBS solution on the β-type ternary and binary alloy samples. From the Mott-Schottky results, it is possible to quantify the donor density (defectivity of the film) of the passive films [58–60].

The Mott-Schottky relationship (Eq. (1)) can be applied to calculate the donor density in the passive layer [58]:

$$C^{-2} = \frac{2\left(E - E_{FB} - \frac{kT}{e}\right)}{\varepsilon\varepsilon_0 e N_d} \quad (1)$$

where C is the capacitance, T is the temperature, k is the Boltzmann constant, E_{FB} is the flat band potential, N_d is the donor density, e is the electron charge, ε_0 is the permittivity of

Table 2 – The fitting values of the equivalent circuit components applied to EIS spectra of Ti–45Nb, 96(Ti–45Nb)-4Ga and 92(Ti–45Nb)-8Ga alloys, potentiostatic pre-passivated at 0.6 V (vs. SCE) in PBS solution.

	R_1 (Ωcm^2)	R_2 ($\Omega cm^2 x10^5$)	CPE_1-Q ($\Omega^{-1}s^n cm^2 x10^{-5}$)	CPE_1-n
Ti–45Nb	32 ± 1	7.1 ± 0.3	1.52 ± 0.12	0.9 ± 0.01
96(Ti–45Nb)-4Ga	32 ± 1	8.2 ± 0.7	1.29 ± 0.02	0.9 ± 0.03
92(Ti–45Nb)-8Ga	33 ± 1	8.2 ± 0.4	1.12 ± 0.03	0.9 ± 0.01

vacuum and $\varepsilon \cong 42$ (for Ti–45Nb (wt.%)) [61] the dielectric constant of the passive films formed on Ti–45Nb. Woldemedhin et al. [24] studied the passivity and characterization of the anodic oxides of Ti–Nb alloys via Mott-Schottky measurements by calculating the dielectric constant of the oxides on electropolished Ti–Nb alloys (Nb content 10 and 20 wt%). The dielectric constant of the Ti–10Nb and Ti–20Nb was calculated as 48.5 and 50.5, respectively. However, in our case, the dielectric constant of the studied alloys was taken as $\varepsilon \cong 42$ which is approximated from the literature for the anodic oxides grown on Ti–Nb binary alloys [61]. The derivative of Eq. (1) with respect to the applied potential is used to calculate donor density (Eq. (2)).

$$\frac{dC^{-2}}{dE} = \frac{2}{\varepsilon\varepsilon_0 e N_d} \quad (2)$$

The capacitance versus the applied potential for the passive films grown at 0.6 V (vs. SCE) in PBS solution is shown in Fig. 7. Measurements were carried out by applying an AC perturbation at a fixed frequency of 1 kHz. A potential range of 1 V (vs. SCE) to −1 V (vs. SCE) was swept with a step size of 50 mV. A linear region, with a positive slope, illustrates an n-type semiconducting behaviour of the passive films. Based on the character of n-type semiconductors, the oxygen vacancies are the dominant charge carriers in the passive film. The slope of the Mott-Schottky plot is inversely related to the defectiveness of the passive films. As a result, the highest slope in the Mott-Schottky plot means the lowest donor density [53,60,62,63].

Mott-Schottky measurements reveal that passive films formed on the studied alloys are n-type semiconductors. The donor densities for the Ti–45Nb, 96(Ti–45Nb)-4Ga and 92(Ti–45Nb)-8Ga are calculated from the slope of the linear region (−0.75 V to −0.25 V (vs. SCE)) of Mott-Schottky plots as 1.25 ± 0.2 x 10^{20} cm^{-3}, 1.19 ± 0.1 x 10^{20} cm^{-3}, 9.04 ± 0.2 x 10^{19} cm^{-3}, respectively. Qin et al. [60] studied the corrosion behaviour of selective laser melted (SLM) Ti–35Nb alloys. The calculated donor densities were in the same magnitude of 10^{19} cm^{-3} under different applied potentiostatic polarization potentials (0.5, 0.75, 1, 1.25, and 1.5 V). In this work, the donor densities are slightly lowered with minor Ga addition. This could be attributed to the incorporation of Ga species into the oxide together with Ti- and Nb-based oxides.

The relationship between alloying elements and the donor density of the passive films can be explained. Elements with higher valence electrons can stabilize the passive film via the elimination of anion vacancies in Ti-based passive films. The presence of Nb^{5+} cations annihilates the anion vacancies to make the passive films more stable and less defective [64]. Thus, due to the presence of a high amount of Nb in the alloys, it is possible to observe similar donor density values with minor Ga additions. However, donor densities are slightly lowered with minor Ga addition. In other words, passive films formed on Ga-containing alloys exhibit a less defective nature with better barrier properties. For Ti–45Nb, the incorporation of Nb species into the Ti oxide lattice yields the formation of mixed (Ti–Nb) oxides [19,20,23,38,65]. Thus, the contribution of Ga species to mixed (Ti–Nb) oxides might yield the formation of mixed (Ti–Nb-Ga) oxides. In this case, it is possible to say that the contribution of Ga species to the passive film does yield a minor positive change in terms of donor densities.

3.3. *Passive film analysis*

X-ray photoelectron spectroscopy (XPS) was performed to comparatively analyze the chemical composition of the

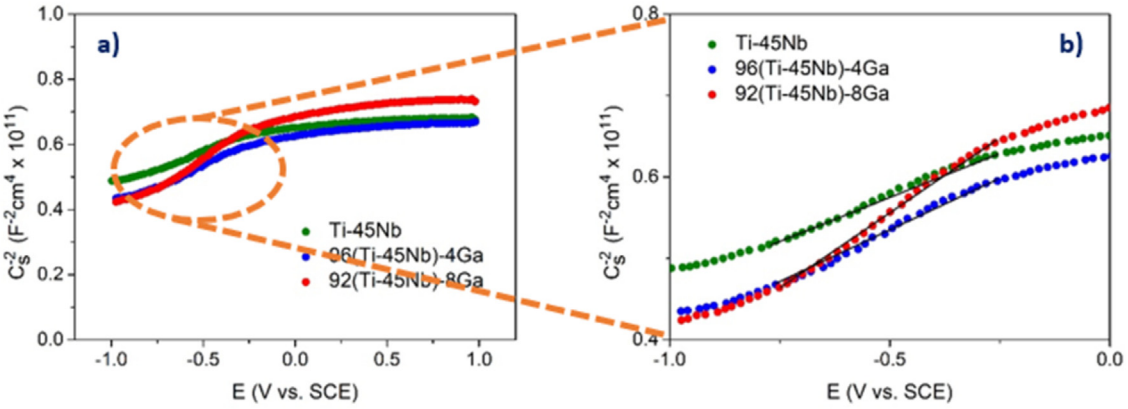

Fig. 7 – a) Mott-Schottky plot (scanned with a potential range of 1 V (vs. SCE) to −1 V (vs. SCE)) for the passive film formed on Ti–45Nb, 96(Ti–45Nb)-4Ga and 92(Ti–45Nb)-8Ga alloys for 1 h at 0.6 V (vs. SCE) in PBS solution. b) Inset to show the linear region of the Mott-Schottky plot.

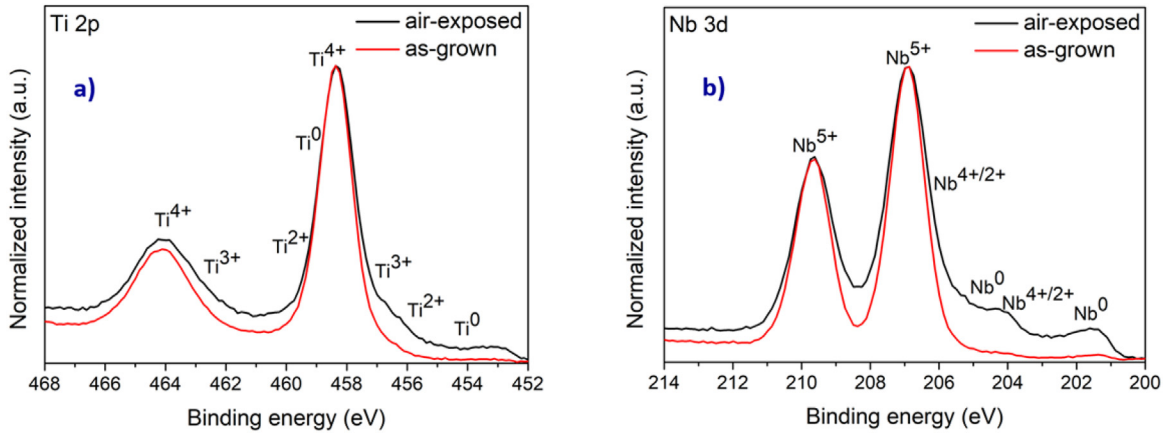

Fig. 8 – Normalized high-resolution XPS spectra of a) Ti 2p and b) Nb 3d for Ti–45Nb alloy, after immersion in PBS solution under anodic potentiostatic polarization conditions (as-grown) at 0.6 V (vs. SCE) for 1 h (air-exposed sample as reference).

passive layers formed on Ti–45Nb and 92(Ti–45Nb)-8Ga alloy samples after immersion in PBS solution under anodic potentiostatic polarization conditions (as-grown) at 0.6 V (vs. SCE) for 1 h (air-exposed samples were used as reference). In order to verify the presence of Ti, Nb, and Ga species in surface-near regions, the corresponding set of detailed spectra for Ti 2p, Nb 3d, and Ga 2p is plotted in Figs. 8 and 9 for Ti–45Nb and 92(Ti–45Nb)-8Ga.

For both alloys, the Ti 2p spectrum consists of $2p_{3/2}$ and $2p_{1/2}$ peaks, and the peaks located at 459 eV and 464 eV are assigned to the Ti^{4+} oxide state. The Nb 3d spectrum gives rise to peaks at 207 eV and 210 eV, which belong to Nb $3d_{5/2}$ and Nb

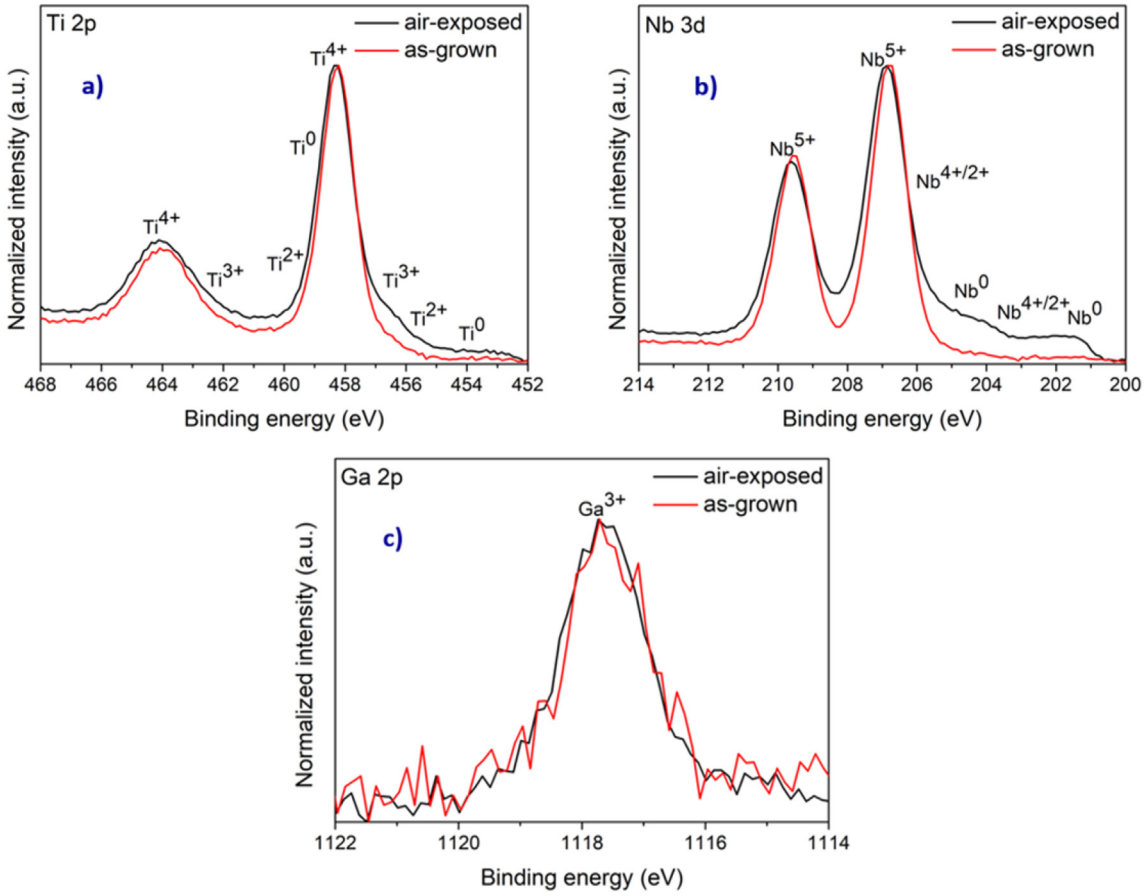

Fig. 9 – Normalized high-resolution XPS spectra of a) Ti 2p, b) Nb 3d, and c) Ga 2p for 92(Ti–45Nb)-8Ga alloy, after immersion in PBS solution under anodic potentiostatic polarization conditions (as-grown) at 0.6 V (vs. SCE) for 1 h (air-exposed sample as reference).

$3d_{3/2}$ electrons from the Nb^{5+} oxide state, respectively. For 92(Ti–45Nb)-8Ga, the Ga 2p spectrum consists of a $2p_{3/2}$ peak only, and the peak is located at 1118 eV which belongs to the Ga^{3+} oxide state [19,23,66,67].

In addition, for both alloys, Ti^0 (metal) peaks at 453 eV and Nb^0 (metal) peaks at 201 eV and 204 eV were observed, Ga^0 (metal) peaks were not observed in Ga 2p high-resolution spectra for 92(Ti–45Nb)-8Ga. However, these metal peaks and side oxide peaks ($Ti^{3+}$and $Nb^{4+/2+}$) are weakly pronounced. In this case, the contribution of the Ti^{4+} and Nb^{5+} oxide states are dominant for the passive film grown on Ti–45Nb. Similarly, the contribution of the Ti^{4+}, Nb^{5+}, and Ga^{3+} oxide states are dominant states for the passive film formed on 92(Ti–45Nb)-8Ga. The main difference between the air-exposed (reference) and the as-grown states is the absence of metal peaks (Ti^0, Nb^0, Ga^0) and low valence state peaks (Ti^{3+} and $Nb^{4+/2+}$) for both alloys under as-grown conditions. The absence of these peaks for as-grown samples represents the enhanced film growth of the highest valence oxide (Ti^{4+}, Nb^{5+}, and Ga^{3+}) via anodically driven passivation [19,23,66]. In addition, for both alloys, the O 1s spectrum (not shown here) was composed of two overlapping peaks at 530 eV and 531 eV for (Ti–45Nb) and (92(Ti–45Nb)-8Ga). The peak at 530 eV is ascribed to the O^{2-} state mainly in the bonding states of Ti, Nb, and Ga-based oxides. The peak at 531 eV is attributed to OH^- bonding [19,23]. As mentioned above in the Mott-Schottky section, the incorporation of Ga species to Ti- and Nb-based oxides might yield the formation of mixed (Ti–Nb-Ga) oxides in the passive film of 92(Ti–45Nb)-8Ga.

3.4. *THP-1 macrophage viability and adhesion*

Generally, high cell viability was observed on macrophages adhered for 24 h on the different materials (Fig. 10), where no significant difference was found between the number of viable cells adhered to the 96(Ti–45Nb)-4Ga, 92(Ti–45Nb)-8Ga, and the control surfaces (Ti–45Nb and cp-Ti).

3.5. Staphylococcus aureus *viability and adhesion*

A significant reduction ($p \leq 0.05$) in viability was observed when *S. aureus* was cultured for 4 h on the 92(Ti–45Nb)-8Ga materials compared to the cp-Ti control. Although not significant, at 4 h a dose-dependent decreasing trend in *S. aureus* viable counts was observed in Ga-containing alloys. At 24 h, the amount of viable *S. aureus* adhered to all four materials was comparable (Fig. 11).

4. Discussion

The β-type Ti–Nb binary alloys receive considerable attention as promising candidates in the development of the next generation of metallic biomaterials, specifically for hard tissue implant applications owing to their excellent mechanical properties and biocompatibility. For improving the antibacterial properties, minor alloying with bactericidal elements is a potential strategy [21,23,68]. In this work, the effect of minor gallium (Ga) addition to Ti–45Nb alloys on the corrosion and

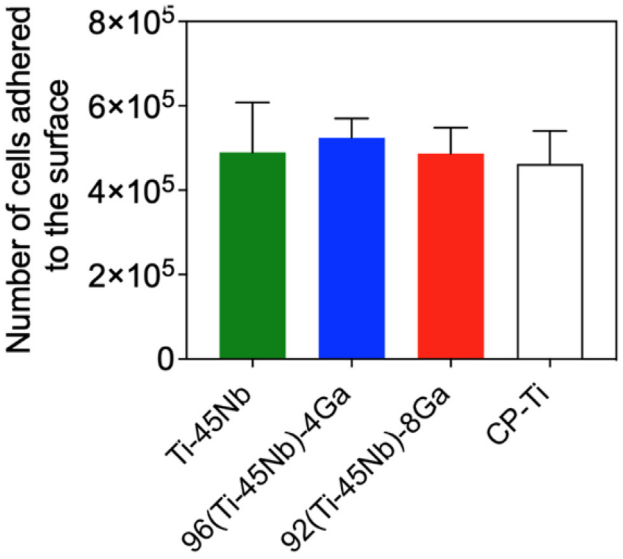

Fig. 10 – The number of viable THP-1 macrophages adhered to the surfaces after 24 h of direct contact with the surface of the alloys, as analyzed by nucleocounter. Data represent the means from three independent experiments (n = 3; ±SD) with duplicate samples. *$p \leq 0.05$ using one-way ANOVA with LSD post-hoc test (between the three β-type Ti–Nb alloys and the cp-Ti).

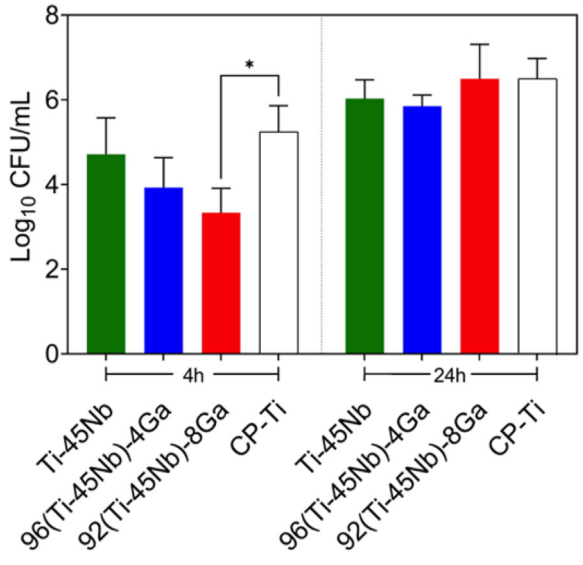

Fig. 11 – Viability of surface adhered *Staphylococcus aureus* ATCC 25923 after 4 h and 24 h cultures measured by viable counting of colony-forming units (CFU). Data represent the means from three independent experiments (n = 3; ±SD) with duplicate samples. *$p \leq 0.05$ using one-way ANOVA with LSD post-hoc test (between the three β-type Ti–Nb alloys) and Dunnett's post-hoc test (between each β-type Ti–Nb alloys and the cp-Ti).

passive film properties, and on the early *in vitro* biological interactions with macrophages and *S. aureus* was investigated.

In terms of overall corrosion response, due to the presence of Ga fractions up to 8 wt% in the solid solution of the β-phase, Ga-containing alloy samples exhibit more positive E_{OCP} and corresponding E_{corr} values compared to the Ti–45Nb reference alloy. In addition, the corrosion current densities for all three alloys are extremely low because of the spontaneous formation of protective passive films [19]. Corresponding metal ion release rates were found to be very low not only for Ti and Nb species but also for Ga ions. In addition, anodic passive current densities are slightly lowered with Ga addition, which is indicative of a more protective nature of the oxide films. Overall, the corrosion response of the studied alloys is similar to (Ti–40Nb)–4In alloy reported by Gebert et al. [19], where they observed similar passivation current densities (3–4 μAcm^{-2}). In addition, corrosion current density values are in agreement with those reported for as-polished Ti–45Nb alloys tested in Ringer's solution [27]. However, the as-cast or as-polished sample state is not suitable for direct implantation into the body. Usually, different surface treatments like blasting, acid etching, or anodic oxidation need to be applied to stimulate bone cell response without altering the corrosion resistance [27,38,69].

This work aimed to understand how Ga species contribute to alloy passivity in addition to Ti- and Nb-based oxides. To this end, potentiostatic polarization, electrochemical impedance spectroscopy (EIS), and Mott-Schottky measurements were performed to investigate the passive film properties. The minor alloy addition of Ga lowers the mean passive current densities after anodic potentiostatic polarization. This indicates that the conductivity/permeability for charge carriers of passive films grown on Ga-containing alloys is lower than Ti–45Nb. Minor Ga addition improves the passive film resistance according to EIS results due to the possible Ga-based oxide contribution to passive film growth together with Ti- and Nb-based oxides [19]. Overall, the electrochemical response of the passive films formed under 0.6 V (vs. SCE) is similar to the passive films formed on Ti–40Nb alloys at 0.6 V (vs. Ag|AgCl) [66]. In addition, for Ga-containing alloys, the reduction in current densities could be attributed to the size of β-grains since grain size affects the electrochemical properties [49]. However, the literature reports different results for the effect of grain size on the corrosion behaviour of titanium alloys, from the higher to the lower corrosion resistance [49–52]. In our case, it might be possible to expect better corrosion and passivity behaviour for Ga-containing alloys due to the grain refinement effect of Ga.

In addition, Mott-Schottky measurements reveal that passive films formed on the studied alloys are n-type semiconductors, like for other Ti alloys where the oxygen vacancies are the dominant charge carriers [60]. The formation energy of a titanium interstitial (4.7 eV) is higher than the needed energy for the generation of an oxygen vacancy (2.7 eV). Thus, the donor population in the passive film is mainly oxygen vacancies. The donor densities (calculated from the slope of the Mott-Schottky plot) are slightly lowered with minor Ga addition to a β-type Ti–45Nb. The passive films formed on Ga-containing alloys exhibit a less defective nature. For Ga-containing alloys, additional incorporation of minor Ga^{3+} species into the oxide lattice does yield a minor but positive effect in terms of donor densities.

From the electronic conductivity viewpoint, the increase in donor density leads to a smaller band gap in passive film (as a metal oxide) by easing electron transfer. In terms of the ionic conductivity view, oxygen vacancies carry ionic charges leading to higher ionic conductivity in the passive film [70]. In our case, the contribution of Ga-based oxides to passive film together with Ti- and Nb-based oxides may yield a formation of a mixed (Ti–Nb-Ga) oxide. Both TiO_2 and Nb_2O_5 are semiconductors with band gaps of around 3.2 and 3.4 eV, respectively [61]. On the other hand, Ga_2O_3 exhibits a wide band gap of around 4.8 eV [71]. The contribution of Ga-based oxides with wide band gaps to passive film growth lowers the electronic conductivity via limiting the electron transfer. Thus, due to the limited electron transfer (low electronic conductivity), the donor densities are lowered (low ionic conductivity) with Ga addition.

XPS measurements on passive films formed in PBS by potentiostatic polarization for 92(Ti–45Nb)-8Ga reveal that the passive layer consists of Ti, Nb, and Ga-based oxides. Our results indicate that on the β-type Ti–Nb-Ga alloy surfaces, Ga species mainly contribute to the passive film formation instead of significant corrosive Ga-ion release. The contribution of Ga^{3+} species to mixed (Ti, Nb)O_2 oxides is assumed to yield the formation of mixed (Ti–Nb-Ga) oxides. In the end, the high corrosion and passive film resistance of Ti–45Nb are retained and even slightly improved with Ga addition. Based on these findings, Ga-containing alloys exhibit better corrosion performance as a biomedical material, compared to Ti–45Nb.

In addition to investigating the corrosion and passivity properties achieved by alloying minor additions of Ga into Ti–45Nb, we have evaluated the initial immune cell attachment and antibacterial properties of the alloys. In particular, we evaluated the *in vitro* adhesion and viability of THP-1 macrophages in direct contact with the surface of the alloys. Macrophages have a critical role in the innate immune response to biomaterials. They are the primary infiltrating cells that respond and interact with other cell types to regulate cytokine and chemokine secretion, cell recruitment, fibrous encapsulation, and finally dictate the outcome of the host response to the biomaterial [72]. In this investigation, we found that the 96(Ti–45Nb)-4Ga and 92(Ti–45Nb)-8Ga alloys support adhesion and viability of THP-1 macrophages at a level comparable to the controls Ti–45Nb and cp-Ti. Since Ga addition contributes to passive film formation without significant corrosion and Ga-ion release, it is not surprising that there are not enough toxic elements released from the alloys that interfere with cellular viability or adhesion. These promising viability results are in line with the previous studies of metallurgical addition of Ga in various amounts (1–2% up to 23% wt.) where no cytotoxicity was observed in human fetal progenitor and human osteosarcoma cell lines [12].

Moreover, the initial *in vitro* antibacterial effect of Ga addition was investigated against *S. aureus*, since it is one of the most common etiologic agents associated with the aseptic failure of implanted orthopaedic devices [73,74]. During early

(4 h) material-bacterial interactions, this study showed that 92(Ti–45Nb)-8Ga significantly decreased *S. aureus* viability compared to the clinically used cp-Ti material. Furthermore, at 4 h, a decreasing trend in *S. aureus* viability was observed with increasing Ga concentrations. As reported by Cochis et al. [12], this mechanism is considered to be a 'trojan-horse' strategy; Ga^{3+} ions are released from the material surface, which can not be reduced, replacing reducible Fe^{3+} in certain metabolic pathways, interfering with *S. aureus* iron-sulfur clusters, and resulting in nutrient limitation, modulation of bacterial metabolism and cell death. Compared to other investigations in which Ga was incorporated into Ti at similar concentrations [12], in this study, we observed a limited antibacterial effect, possibly due to the observed contribution of Ga to the passive film and the marginal release of Ga even after 7 days. This is not surprising, as this passivity likely reduces the ability of alloyed Ga to release into the media and interact with surface-adhered bacteria.

5. Summary and conclusions

In this work, the role of minor gallium (Ga) addition on the corrosion, passivity, and antibacterial properties of β-type Ti–45Nb alloys was investigated in a phosphate buffer saline (PBS) solution.

- XRD and SEM results reveal that all studied alloys displayed a β-phase structure with no diffraction peaks belonging to secondary phases due to the higher stabilizing effect of Nb on the β-phase.
- In terms of corrosion response, all alloys exhibit self-passivation without passive layer breakdown. The minor Ga addition slightly reduces the corrosion and passivation current densities.
- Ga addition improves the passive film resistance due to the possible Ga-based oxide contribution to passive film growth together with Ti- and Nb-based oxides. In addition, Mott-Schottky measurements show that passive films formed on the studied alloys are n-type semiconductors, and Ga addition does yield a minor positive effect on the donor density of the passive films. However, in terms of overall electrochemical response, it is not possible to observe a direct trend with Ga additions, but Ga-containing alloys exhibit a better passivation response compared to Ti–45Nb.
- XPS measurements for 92(Ti–45Nb)-8Ga show that the passive layer consists of Ti-, Nb-, and Ga-based oxides. The contribution of Ga species to Ti- and Nb-based oxides might yield the formation of mixed (Ti–Nb-Ga) oxides. In addition, a very low Ga release rate was confirmed under free corrosion conditions. Therefore, it can be assumed that Ga species may contribute to passive film formation on Ga-containing alloy surfaces.
- The addition of 8 wt% Ga into Ti–45Nb showed antibacterial properties against *S. aureus* compared to cp-Ti after the early interaction period of 4 h. In addition, all tested materials showed good viability of THP-1 macrophage-like cells adhered to the surfaces for 24 h *in vitro*.

In conclusion, the high corrosion and passive film resistance of Ti–45Nb are retained and even slightly improved with minor Ga addition. Based on these findings and compared with Ti–45Nb, Ga-containing alloys exhibit slightly better corrosion performance, minor initial antibacterial properties, and favourable immune cell cytocompatibility, suggesting a potential application as a biomedical material. However, further *in vitro* and *in vivo* studies should be carried out to understand the biological interactions with these novel biomaterials.

Funding information

All authors are grateful for the financial support from the European Commission within the H2020-MSCA grant agreement no. 861046 (BIOREMIA-ETN). Additional funding is provided by the Deutsche Forschungsgemeinschaft (DFG) under project GE/1106/12–1, the Swedish Research Council (2022–00853, 2020–04715), the Swedish state under the agreement between the Swedish government and the country councils, the ALF-agreement (ALFGBG-978896, ALFGBG-72564), the Hjalmar Svensson Foundation, the Doctor Felix Neubergh Foundation, and the Adlerbertska Foundation. The funding sources had no role in the conceptualization, design, data collection, analysis, decision to publish, or preparation of the manuscript.

Declaration of competing interest

The authors declare the following financial interests/personal relationships which may be considered as potential competing interests: Adnan Akman reports financial support was provided by European Commission.

Acknowledgements

The authors are grateful to Stefan Pilz for fruitful scientific discussions and grateful to Andrea Voβ for chemical analysis.

REFERENCES

[1] Guo Z, Huang Y, Sun C, He Z, Yuan D, Cai B, et al. Ti–Mo–Zr alloys for bone repair: mechanical properties, corrosion resistance, and biological performance. J Mater Res Technol 2023;24:7624–37. https://doi.org/10.1016/j.jmrt.2023.05.006.

[2] Li Y, Yang C, Zhao H, Qu S, Li X, Li Y. New developments of ti-based alloys for biomedical applications. Materials 2014;7(3):1709–800. https://doi.org/10.3390/ma7031709.

[3] Miura K, Yamada N, Hanada S, Jung TK, Itoi E. The bone tissue compatibility of a new Ti-Nb-Sn alloy with a low Young's modulus. Acta Biomater 2011;7(5):2320–6. https://doi.org/10.1016/j.actbio.2011.02.008.

[4] Hussein MA, Azeem MA, Kumar AM, Saravanan S, Ankah N, Sorour AA. Design and processing of near-β Ti–Nb–Ag alloy with low elastic modulus and enhanced corrosion resistance for orthopedic implants. J Mater Res Technol 2023;24:259–73. https://doi.org/10.1016/j.jmrt.2023.03.003.

[5] Gomes CC, Moreira LM, Santos VJSV, Ramos AS, Lyon JP, Soares CP, et al. Assessment of the genetic risks of a metallic alloy used in medical implants. Genet Mol Biol 2011;34(1):116–21. https://doi.org/10.1590/S1415-47572010005000118.
[6] Fischer M, Joguet D, Robin G, Peltier L, Laheurte P. In situ elaboration of a binary Ti-26Nb alloy by selective laser melting of elemental titanium and niobium mixed powders. Mater Sci Eng C 2016;62:852–9. https://doi.org/10.1016/j.msec.2016.02.033.
[7] Monteiro E dos S, Moura de Souza Soares F, Nunes LF, Carvalho Santana AI, Sérgio de Biasi R, Elias CN. Comparison of the wettability and corrosion resistance of two biomedical Ti alloys free of toxic elements with those of the commercial ASTM F136 (Ti–6Al–4V) alloy. J Mater Res Technol 2020;9(6):16329–38. https://doi.org/10.1016/j.jmrt.2020.11.068.
[8] Zhao Z, Xu W, Xin H, Yu F. Microstructure, corrosion and anti-bacterial investigation of novel Ti-xNb-yCu alloy for biomedical implant application. J Mater Res Technol 2022;18:5212–25. https://doi.org/10.1016/j.jmrt.2022.04.158.
[9] Souza JGS, Bertolini MM, Costa RC, Nagay BE, Dongari-Bagtzoglou A, Barão VAR. Targeting implant-associated infections: titanium surface loaded with antimicrobial. iScience 2021;24(1). https://doi.org/10.1016/j.isci.2020.102008.
[10] Svensson Malchau K, Tillander J, Zaborowska M, Hoffman M, Lasa I, Thomsen P, et al. Biofilm properties in relation to treatment outcome in patients with first-time periprosthetic hip or knee joint infection. J Orthop Transl 2021;30(May):31–40. https://doi.org/10.1016/j.jot.2021.05.008.
[11] Rzhepishevska O, Ekstrand-Hammarström B, Popp M, Björn E, Bucht A, Sjöstedt A, et al. The antibacterial activity of Ga3+ is influenced by ligand complexation as well as the bacterial carbon source. Antimicrob Agents Chemother 2011;55(12):5568–80. https://doi.org/10.1128/AAC.00386-11.
[12] Cochis A, Azzimonti B, Chiesa R, Rimondini L, Gasik M. Metallurgical gallium additions to titanium alloys demonstrate a strong time-increasing antibacterial activity without any cellular toxicity. ACS Biomater Sci Eng 2019. https://doi.org/10.1021/acsbiomaterials.9b00147.
[13] Li L, Chen Y, Lu Y, Qin S, Huang G, Huang T, et al. Effect of heat treatment on the corrosion resistance of selective laser melted Ti6Al4V3Cu alloy. J Mater Res Technol 2021;12:904–15. https://doi.org/10.1016/j.jmrt.2021.03.041.
[14] Hijazi S, Visaggio D, Pirolo M, Frangipani E, Bernstein L, Visca P. Antimicrobial activity of gallium compounds on ESKAPE pathogens. Front Cell Infect Microbiol 2018;8(SEP):1–11. https://doi.org/10.3389/fcimb.2018.00316.
[15] Goss CH, Kaneko Y, Khuu L, Anderson GD, Ravishankar S, Aitken ML, et al. Gallium disrupts bacterial iron metabolism and has therapeutic effects in mice and humans with lung infections. Sci Transl Med 2018;10(460):1–12. https://doi.org/10.1126/scitranslmed.aat7520.
[16] Minandri F, Bonchi C, Frangipani E, Imperi F, Visca P. Promises and failures of gallium as an antibacterial agent. Future Microbiol 2014;9(3):379–97. https://doi.org/10.2217/fmb.14.3.
[17] Kaneko Y, Thoendel M, Olakanmi O, Britigan BE, Singh PK. The transition metal gallium disrupts Pseudomonas aeruginosa iron metabolism and has antimicrobial and antibiofilm activity. J Clin Invest 2007;117(4):877–88. https://doi.org/10.1172/JCI30783.
[18] Hanada S, Matsumoto H, Watanabe S. Mechanical compatibility of titanium implants in hard tissues. Int. Congr. Ser. 2005;1284:239–47. https://doi.org/10.1016/j.ics.2005.06.084.
[19] Gebert A, Oswald S, Helth A, Voss A, Gostin PF, Rohnke M, et al. Effect of indium (In) on corrosion and passivity of a beta-type Ti-Nb alloy in Ringer's solution. Appl Surf Sci 2015;335:213–22. https://doi.org/10.1016/j.apsusc.2015.02.058.
[20] Alberta LA, Vishnu J, Hariharan A, Pilz S, Gebert A, Calin M. Novel low modulus beta-type Ti-Nb alloys by gallium and copper minor additions for antibacterial implant applications. J Mater Res Technol 2022;20:3306–22. https://doi.org/10.1016/j.jmrt.2022.08.111.
[21] Calin M, Helth A, Gutierrez Moreno JJ, Bönisch M, Brackmann V, Giebeler L, et al. Elastic softening of β-type Ti-Nb alloys by indium (In) additions. J Mech Behav Biomed Mater 2014;39:162–74. https://doi.org/10.1016/j.jmbbm.2014.07.010.
[22] Bönisch M, Calin M, Waitz T, Panigrahi A, Zehetbauer M, Gebert A, et al. Thermal stability and phase transformations of martensitic Ti-Nb alloys. Sci Technol Adv Mater 2013;14(5). https://doi.org/10.1088/1468-6996/14/5/055004.
[23] Helth A, Gostin PF, Oswald S, Wendrock H, Wolff U, Hempel U, et al. Chemical nanoroughening of Ti40Nb surfaces and its effect on human mesenchymal stromal cell response. J Biomed Mater Res - Part B Appl Biomater 2014;102(1):31–41. https://doi.org/10.1002/jbm.b.32976.
[24] Woldemedhin MT, Raabe D, Hassel AW. Characterization of thin anodic oxides of Ti-Nb alloys by electrochemical impedance spectroscopy. Electrochim Acta 2012;82:324–32. https://doi.org/10.1016/j.electacta.2012.06.029.
[25] Bai YJ, Wang YB, Cheng Y, Deng F, Zheng YF, Wei SC. Comparative study on the corrosion behavior of Ti-Nb and TMA alloys for dental application in various artificial solutions. Mater Sci Eng C 2011;31(3):702–11. https://doi.org/10.1016/j.msec.2010.12.010.
[26] Woldemedhin MT, Raabe D, Hassel AW. Anodic oxides on a beta type Nb-Ti alloy and their characterization by electrochemical impedance spectroscopy. Phys. Status Solidi Appl. Mater. Sci. 2010;207(4):812–6. https://doi.org/10.1002/pssa.200983324.
[27] Gostin PF, Helth A, Voss A, Sueptitz R, Calin M, Eckert J, et al. Surface treatment, corrosion behavior, and apatite-forming ability of ti-45Nb implant alloy. J Biomed Mater Res - Part B Appl Biomater 2013;101(2):269–78. https://doi.org/10.1002/jbm.b.32836.
[28] Woldemedhin MT, Raabe D, Hassel AW. Grain boundary electrochemistry of β-type Nb-Ti alloy using a scanning droplet cell. Phys. Status Solidi Appl. Mater. Sci. 2011;208(6):1246–51. https://doi.org/10.1002/pssa.201000991.
[29] Çaha I, Alves A, Chirico C, Pinto A, Tsipas S, Gordo E, et al. Corrosion and tribocorrosion behavior of Ti-40Nb and Ti-25Nb-5Fe alloys processed by powder metallurgy. Metall Mater Trans A Phys Metall Mater Sci 2020;51(6):3256–67. https://doi.org/10.1007/s11661-020-05757-6.
[30] Okazaki Y. A new Ti-15Zr-4Nb-4Ta alloy for medical applications. Curr Opin Solid State Mater Sci 2001;5(1):45–53. https://doi.org/10.1016/S1359-0286(00)00025-5.
[31] Godley R, Starosvetsky D, Gotman I. Corrosion behavior of a low modulus β-Ti-45%Nb alloy for use in medical implants. J Mater Sci Mater Med 2006;17(1):63–7. https://doi.org/10.1007/s10856-006-6330-6.
[32] Virtanen S, Milošev I, Gomez-Barrena E, Trebše R, Salo J, Konttinen YT. Special modes of corrosion under physiological and simulated physiological conditions. Acta Biomater 2008;4(3):468–76. https://doi.org/10.1016/j.actbio.2007.12.003.
[33] Balamurugan A, Rajeswari S, Balossier G, Rebelo AHS, Ferreira JMF. Corrosion aspects of metallic implants - an overview. Mater Corros 2008;59(11):855–69. https://doi.org/10.1002/maco.200804173.
[34] Raman V, Nagarajan S, Rajendran N. Electrochemical impedance spectroscopic characterisation of passive film

formed over β Ti-29Nb-13Ta-4.6Zr alloy. Electrochem Commun 2006;8(8):1309–14. https://doi.org/10.1016/j.elecom.2006.06.004.
[35] Martins DQ, Osório WR, Souza MEP, Caram R, Garcia A. Effects of Zr content on microstructure and corrosion resistance of Ti-30Nb-Zr casting alloys for biomedical applications. Electrochim Acta 2008;53(6):2809–17. https://doi.org/10.1016/j.electacta.2007.10.060.
[36] Geetha M, Kamachi Mudali U, Gogia AK, Asokamani R, Raj B. Influence of microstructure and alloying elements on corrosion behavior of Ti-13Nb-13Zr alloy. Corrosion Sci 2004;46(4):877–92. https://doi.org/10.1016/S0010-938X(03)00186-0.
[37] Hariharan A, Goldberg P, Gustmann T, Maawad E, Pilz S, Schell F, et al. Designing the microstructural constituents of an additively manufactured near β Ti alloy for an enhanced mechanical and corrosion response. Mater Des 2022;217:110618. https://doi.org/10.1016/j.matdes.2022.110618.
[38] Gebert A, Eigel D, Gostin PF, Hoffmann V, Uhlemann M, Helth A, et al. Oxidation treatments of beta-type Ti-40Nb for biomedical use. Surf Coatings Technol 2016;302:88–99. https://doi.org/10.1016/j.surfcoat.2016.05.036.
[39] Ridzwan MIZ, Shuib S, Hassan AY, Shokri AA, Mohammad Ibrahim MN. Problem of stress shielding and improvement to the hip implant designs: a review. J Med Sci 2007;7(3):460–7. https://doi.org/10.3923/jms.2007.460.467.
[40] Andrea L, Vishnu J, Douest Y, Perrin K, Trunfio-sfarghiu A, Courtois N, et al. Tribology international tribocorrosion behavior of β -type Ti-Nb-Ga alloys in a physiological solution. Tribol Int 2023 January;181:108325. https://doi.org/10.1016/j.triboint.2023.108325.
[41] Alberta LA, Fortouna Y, Vishnu J, Pilz S, Gebert A, Lekka C, et al. Effects of Ga on the structural, mechanical and electronic properties of β-Ti-45Nb alloy by experiments and ab initio calculations. J Mech Behav Biomed Mater 2023 February;140:105728. https://doi.org/10.1016/j.jmbbm.2023.105728.
[42] Dos Santos RF, Rossi MC, Vidilli AL, Amigó Borrás V, Afonso CRM. Assessment of β stabilizers additions on microstructure and properties of as-cast β Ti-Nb based alloys. J Mater Res Technol 2023;22:3511–24. https://doi.org/10.1016/j.jmrt.2022.12.144.
[43] Bratsch SG. Standard electrode potentials and temperature coefficients in water at 298.15 K. J Phys Chem Ref Data 1989;18(1):1–21. https://doi.org/10.1063/1.555839.
[44] Milazzo G, Caroli S, Braun RD. Tables of standard electrode potentials. J Electrochem Soc 1978;125(6):261C. https://doi.org/10.1149/1.2131790.
[45] Yi G, Liu X, Zheng C, Zhang H, Xu C, Cui YW, et al. Characteristics of passive films formed on As-Cast Ti–6Al-4V in Hank's solution before and after transpassivation. Front Mater 2021 February;7:1–11. https://doi.org/10.3389/fmats.2020.640081.
[46] Pourbaix M, Zhang H, Pourbaix A. Presentation of an Atlas of chemical and electrochemical equilibria in the presence of a gaseous phase. Mater Sci Forum 1997;251(254):143–8. https://doi.org/10.4028/www.scientific.net/msf.251-254.143.
[47] Metikoš-Huković M, Zevnik C. Determination of Polarization resistance and corrosion rate by using pulse method, polarization curves and AAS. Mater Corros 1982;33(12):661–8. https://doi.org/10.1002/maco.19820331204.
[48] Lohrengel MM. Thin anodic oxide layers on aluminium and other valve metals: high field regime. Mater Sci 1993;12:243–94.
[49] Ralston KD, Birbilis N, Davies CHJ. Revealing the relationship between grain size and corrosion rate of metals. Scripta Mater 2010;63(12):1201–4. https://doi.org/10.1016/j.scriptamat.2010.08.035.
[50] Garbacz H, Pisarek M, Kurzydłowski KJ. Corrosion resistance of nanostructured titanium. Biomol Eng 2007;24(5):559–63. https://doi.org/10.1016/j.bioeng.2007.08.007.
[51] Balyanov A, Kutnyakova J, Amirkhanova NA, V Stolyarov V, Valiev RZ. Corrosion resistance of ultra fine-grained Ti 2004;51:225–9. https://doi.org/10.1016/j.scriptamat.2004.04.011.
[52] Hoseini M, Shahryari A, Omanovic S, Szpunar JA. Comparative effect of grain size and texture on the corrosion behaviour of commercially pure titanium processed by equal channel angular pressing. Corrosion Sci 2009;51(12):3064–7. https://doi.org/10.1016/j.corsci.2009.08.017.
[53] Chen LY, Zhang HY, Zheng C, Yang HY, Qin P, Zhao C, et al. Corrosion behavior and characteristics of passive films of laser powder bed fusion produced Ti–6Al–4V in dynamic Hank's solution. Mater Des 2021;208:109907. https://doi.org/10.1016/j.matdes.2021.109907.
[54] Qin P, Chen LY, Liu YJ, Jia Z, Liang SX, Zhao CH, et al. Corrosion and passivation behavior of laser powder bed fusion produced Ti-6Al-4V in static/dynamic NaCl solutions with different concentrations. Corros Sci 2021 May;191:109728. https://doi.org/10.1016/j.corsci.2021.109728.
[55] Fushimi K, Takabatake Y, Nakanishi T, Hasegawa Y. Microelectrode techniques for corrosion research of iron. Electrochim Acta 2013;113:741–7. https://doi.org/10.1016/j.electacta.2013.03.021.
[56] Yanagisawa K, Nakanishi T, Hasegawa Y, Fushimi K. Passivity of dual-phase carbon steel with ferrite and martensite phases in pH 8.4 boric acid-borate buffer solution. J Electrochem Soc 2015;162(7):C322–6. https://doi.org/10.1149/2.0471507jes.
[57] Marcelin S, Ter-Ovanessian B, Normand B. Electronic properties of passive films from the multi-frequency Mott-Schottky and power-law coupled approach. Electrochem Commun 2016;66:62–5. https://doi.org/10.1016/j.elecom.2016.03.003.
[58] Yilmaz A, Traka K, Pletincx S, Hauffman T, Sietsma J, Gonzalez-Garcia Y. Effect of microstructural defects on passive layer properties of interstitial free (IF) ferritic steels in alkaline environment. Corrosion Sci 2021;182:109271. https://doi.org/10.1016/j.corsci.2021.109271. January.
[59] Wang L, Yu H, Wang S, Chen B, Wang Y, Fan W, et al. Quantitative analysis of local fine structure on diffusion of point defects in passive film on Ti. Electrochim Acta 2019;314:161–72. https://doi.org/10.1016/j.electacta.2019.05.048.
[60] Qin P, Chen LY, Zhao CH, Liu YJ, Cao CD, Sun H, et al. Corrosion behavior and mechanism of selective laser melted Ti35Nb alloy produced using pre-alloyed and mixed powder in Hank's solution. Corros Sci 2021 May:189. https://doi.org/10.1016/j.corsci.2021.109609.
[61] Mardare AI, Savan A, Ludwig A, Wieck AD, Hassel AW. High-throughput synthesis and characterization of anodic oxides on Nb-Ti alloys. Electrochim Acta 2009;54(25):5973–80. https://doi.org/10.1016/j.electacta.2009.02.104.
[62] Cheng J, Li J, Yu S, Du Z, Dong F, Zhang J, et al. Corrosion behavior of As-Cast Ti–10Mo–6Zr–4Sn–3Nb and Ti–6Al–4B in hank's solution: A comparison investigation. Metals (Basel) 2021;11(1):1–15. https://doi.org/10.3390/met11010011.
[63] Gai X, Bai Y, Li J, Li S, Hou W, Hao Y, et al. Electrochemical behaviour of passive film formed on the surface of Ti-6Al-4V alloys fabricated by electron beam melting. Corros Sci 2018;145:80–9. https://doi.org/10.1016/j.corsci.2018.09.010.
[64] Metikoš-Huković M, Kwokal A, Piljac J. The influence of niobium and vanadium on passivity of titanium-based implants in physiological solution. Biomaterials 2003;24(21):3765–75. https://doi.org/10.1016/S0142-9612(03)00252-7.

[65] Herzer R, Gebert A, Hempel U, Hebenstreit F, Oswald S, Damm C, et al. Rolled-Up Metal Oxide Microscaffolds to Study Early Bone Formation at Single Cell Resolution. Small 2021;17(12). https://doi.org/10.1002/smll.202005527.
[66] Çaha I, Alves AC, Chirico C, Maria Pinto A, Tsipas S, Gordo E, et al. Atomic–scale investigations of passive film formation on Ti-Nb alloys. Appl Surf Sci 2023;615 (December 2022): 156282. https://doi.org/10.1016/j.apsusc.2022.156282.
[67] Rodríguez CIM, Álvarez MÁL, Rivera J de JF, Arízaga GGC, Michel CR. α-Ga 2 O 3 as a photocatalyst in the degradation of malachite green. ECS J. Solid State Sci. Technol. 2019;8(7):Q3180–6. https://doi.org/10.1149/2.0351907jss.
[68] Kim HY, Ohmatsu Y, Kim J, Hosoda H, Miyazaki S. Mechanical properties and shape memory behavior of Ti-Mo-Ga alloys. Mater Trans 2004;45(4):1090–5. https://doi.org/10.2320/matertrans.45.1090.
[69] Pilz S, Gebert A, Voss A, Oswald S, Göttlicher M, Hempel U, et al. Metal release and cell biological compatibility of beta-type Ti-40Nb containing indium. J Biomed Mater Res - Part B Appl Biomater 2018;106(5):1686–97. https://doi.org/10.1002/jbm.b.33976.
[70] Wang J, Wang Z, Huang B, Ma Y, Liu Y, Qin X, et al. Oxygen vacancy induced band-gap narrowing and enhanced visible light photocatalytic activity of ZnO. ACS Appl Mater Interfaces 2012;4(8):4024–30. https://doi.org/10.1021/am300835p.
[71] Chung Y, Lee C-W. Electrochemistry of gallium. J. Electrochem. Sci. Technol. 2013;4(1):1–18. https://doi.org/10.5229/jecst.2013.4.1.1.
[72] Liu Y, Segura T. Biomaterials-mediated regulation of macrophage cell fate. Front Bioeng Biotechnol 2020;8:1–14. https://doi.org/10.3389/fbioe.2020.609297. December.
[73] Benito N, Mur I, Ribera A, Soriano A, Rodríguez-Pardo D, Sorlí L, et al. The different microbial etiology of prosthetic joint infections according to route of acquisition and time after prosthesis implantation, including the role of multidrug-resistant organisms. J Clin Med 2019;8(5). https://doi.org/10.3390/jcm8050673.
[74] Campoccia D, Montanaro L, Arciola CR. The significance of infection related to orthopedic devices and issues of antibiotic resistance. Biomaterials 2006;27(11):2331–9. https://doi.org/10.1016/j.biomaterials.2005.11.044.